Partially-Blocked Near-Field Sensing: Joint Source DoA and Blockage Range Estimation

Jiaqi Xu*, Björn Ottersten[†], and A. Lee Swindlehurst*

* Center for Pervasive Communications and Computing, University of California, Irvine, CA, USA.

† Interdisciplinary Centre for Security, Reliability and Trust, University of Luxembourg, Luxembourg.

{xu.jiaqi, swindle}@uci.edu, bjorn.ottersten@uni.lu.

Abstract—A diffraction-based channel model is developed for characterizing the line-of-sight channel where the receive array is partially blocked by near-field obstacles. An analytic receive signal model is established where the range and size parameters of the blockage are explicitly modeled in the array steering vector. Based on the proposed model, we consider the joint estimation of the direction of arrivals (DoAs) of impinging RF signals and the parameters of interest for the blockage. General analytical expressions are derived for the Cramér-Rao bounds (CRBs) of both the source-dependent parameters and environmental (common) parameters using both deterministic and stochastic maximum likelihood models. Finally, a Newton's method-based approach is developed to optimize the maximum likelihood criterion to obtain estimates of the DoAs and blockage range of the sensing problem. Numerical results reveal that the maximum likelihood estimates for the DoAs and the blockage range attain the CRB for the stochastic model.

I. Introduction

Accurate modeling of propagation channels is fundamental in wireless communications, radar sensing, and signal processing, as it directly impacts system design and parameter estimation. Traditional channel models often assume unobstructed paths or incorporate multipath propagation, capturing reflections and scattering phenomena in the environment. However, obstacles within the near-field region of the receive array can partially block the array, introducing diffraction effects that significantly alter the characteristics of the received signal [1]. Partial blockages present unique challenges in channel modeling, particularly affecting the estimation of critical parameters such as the direction of arrival (DoA) of impinging signals. At the same time, partial blockages also allow the sensing of the obstruction such as its range from the array and its size. Existing models often neglect the diffraction effects caused by such blockages and rely on simple shadow- or mask-based functions, effectively zeroing out the received signal outside the "visible regions" [2, (79)]. This limitation hinders precise parameter estimation as valuable geometrical information is lost when diffraction is ignored. To address these challenges, we develop a diffraction-based channel model that explicitly incorporates the signal diffraction of partial blockage on the array steering vector. Based on the blockage's range and shape

This work was supported by the U.S. National Science Foundation under grants CCF-2225575, Grant CCF-2322191, and in part, by the Luxembourg National Research Fund (FNR), grant reference IN-TER/MOBILITY/2023/IS/18014377/MCR.

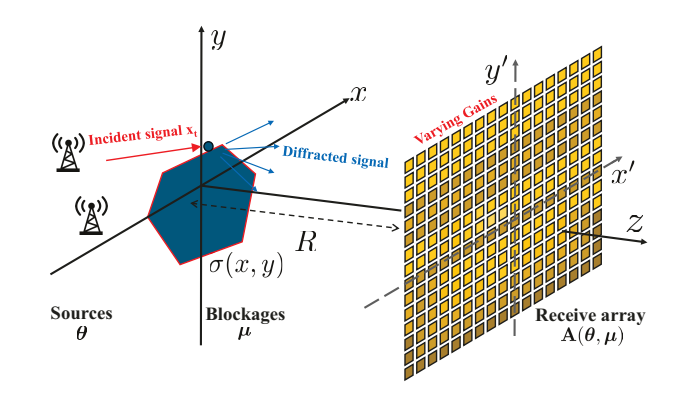


Fig. 1. Illustration of the considered scenario.

parameters, we derive analytical signal models that capture the diffraction phenomenon with closed-form expressions. Our proposed model enables a more accurate representation of partially-blocked channels and facilitates the joint estimation of source DoAs and blockage parameters.

Building upon established maximum likelihood estimation techniques in array signal processing [3], [4], we derive general analytical expressions for the Cramér-Rao bounds (CRBs) of both the source-dependent parameters and environmental (common) parameters. We consider both deterministic and stochastic maximum likelihood models, providing fundamental limits on the estimation accuracy achievable in environments with partial blockages. Furthermore, we implement maximum likelihood estimations for the DoAs of signals in the environment and the blockage range using a multidimensional Newton's search. Numerical simulations demonstrate that the proposed estimators attain the stochastic CRBs when initialized close to the true parameter values, validating the effectiveness of our model and estimation approach.

II. SIGNAL DIFFRACTION MODELING

As illustrated in Fig. 1, we consider a scenario where multiple far-field sources are transmitting signals to a multiantenna receive array while the line-of-sight (LOS) paths are partially occluded by blockages. Exploiting the gain and phase variations of the received signals across the array allows the joint estimation of the DoAs of these sources and the parameters associated with the blockages. Suppose we have K narrowband far-field signal sources with DoAs $\theta_1, \cdots, \theta_M$, where $\theta_k = (\theta_{xk}, \theta_{yk})$ is the DoAs vector with azimuth and elevation components for the kth source. We assume an M-antenna receive array, so that the $M \times 1$ received signal vector can be expressed as follows:

$$\mathbf{s}(t) = \mathbf{A}(\boldsymbol{\theta}, \boldsymbol{\mu})\mathbf{x}(t) + \mathbf{n}(t) , \qquad (1)$$

where $\mathbf{A} = [\mathbf{a}(\boldsymbol{\theta}_1, \boldsymbol{\mu}), \cdots \mathbf{a}(\boldsymbol{\theta}_K, \boldsymbol{\mu})]$ is the $M \times K$ array steering matrix, $\boldsymbol{\theta}$ contains the DoA parameters of the sources, $\boldsymbol{\mu}$ contains the environmental parameters of interest, potentially including the ranges, locations, and shape parameters of the blockages, \mathbf{x} contains the signals transmitted by the sources, and $\mathbf{n} \sim \mathcal{CN}(0, \sigma \mathbf{I}_M)$ is spatially white noise (\mathbf{I}_M is the $M \times M$ identity matrix) with variance σ .

In this work, we will consider the case of a single planar blockage located within the x-y plane of the blockage's coordinate system. The signal sources are located in the far field of the blockages and the array, with z coordinates satisfying $z\ll 0$ and the receive antenna array is located in the plane parallel to the blockage at z=R, where R is the distance of the blockage from the array. For convenience, we define a scaled coordinate system where $u=\sqrt{\frac{2}{\lambda R}}x$ and $v=\sqrt{\frac{2}{\lambda R}}y$, and λ is the wavelength of the signal. In the plane z=0 where the blockage lies, let Ω denote the region occupied by the blockage. Using the scaled coordinates, the cross-section of the blockage is defined by

$$\sigma(u,v) = \begin{cases} 0 & \text{if } (u,v) \in \Omega, \\ 1 & \text{otherwise.} \end{cases}$$
 (2)

Note that (2) only indicates that the signal strength is zero within Ω at z=0. After being diffracted by the blockage, the signal received at the receive array will exhibit a different gain variation pattern. We use (x'_m, y'_m) to denote the coordinates of the mth receive antenna. Similarly, we introduce scaled coordinate in the receiver's coordinate system: $u'_m = \sqrt{\frac{2}{\lambda R}} x'_m$ and $v'_m = \sqrt{\frac{2}{\lambda R}} y'_m$.

According to the Hugyens-Fresnel principle [5], the *m*th element of the array steering vector that captures the signal diffraction can be formulated as follows:

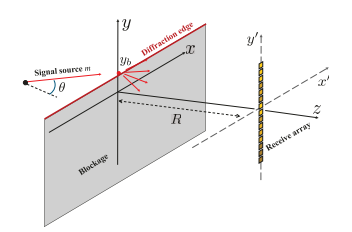
$$\mathbf{a}(\boldsymbol{\theta}_{k}, \boldsymbol{\mu}) = [f_{c}(u'_{m}, v'_{m}) + j f_{s}(u'_{m}, v'_{m})] \times e^{jk_{0}(x'_{m} \sin \theta_{x} + y'_{m} \sin \theta_{y})}, \quad (3)$$

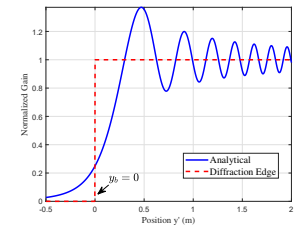
where k_0 denotes the wave number of the signal and

$$f_c(u',v') = \frac{1}{2} \iint_{-\infty}^{\infty} \sigma(u,v) \cos\left[\frac{\pi}{2}(u-u')^2 + \frac{\pi}{2}(v-v')^2\right] du dv'$$

$$(4)$$

$$f_s(u',v') = \frac{1}{2} \iint_{-\infty}^{\infty} \sigma(u,v) \sin\left[\frac{\pi}{2} (u-u')^2 + \frac{\pi}{2} (v-v')^2\right] du dv'$$
(5)





- (a) Blockage illustration.
- (b) Analytical gain variation.

Fig. 2. Diffraction pattern of a straight edge.

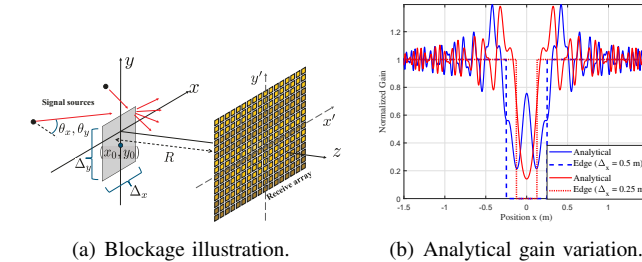


Fig. 3. Diffraction pattern of a rectangle.

are the Fresnel integrals associated with the cross-section function $\sigma(u,v)$. Note that the environmental parameters μ enter the definition of the steering vector in (3) through cross-section function $\sigma(u,v)$ and the range R.

III. TWO CASE STUDIES

In the following, we give examples of partially-blocked channels for two different array configurations and blockage types.

A. Diffraction from a straight edge

Here, we assume the blockage is due to a semi-infinite screen located at z=0. In this case, the vector of parameters reduces to $\mu=\{y_b,R\}$, where y_b is the y-coordinate of the diffraction edge and R is the blockage range. Here, (3) reduces to a simpler form:

$$\mathbf{a}_{m}(y_{b}, R, \theta) = F\left[\left(\sin \theta - \frac{y_{b} - y'_{m}}{r_{m}}\right)\sqrt{\frac{\pi r_{n}}{\lambda}}\right] e^{jky'_{m}\sin \theta}, (6)$$

where $F(u)=\sqrt{\frac{2}{\pi}}\int_u^\infty e^{-jv^2}\mathrm{d}v$ is the complex Fresnel integral, $r_m=\sqrt{(y_b-y_m')^2+R^2}$ is the distance from the mth receive antenna to the edge of the blockage, and y_m' is the coordinate of the mth receive antenna. In Fig. 2(b), we plot the amplitude of the received signal gain \mathbf{a}_m for a straight edge at $y_b=0$ and one signal source with $\theta=(0,0)$ for a carrier frequency of 10 GHz and R=10 m. We see that, due to diffraction effect, the signal power gradually increases when passing the shadow edge, then oscillates around the baseline value. According to (6), the position of the peak gain and the oscillation frequency depend on R.

B. Diffraction of a Rectangular Screen

In this example, we consider a rectangular object with width Δ_x and height Δ_y and centered at $(x_0,y_0,0)$, as shown in Fig. 3(a). In this case, the blockage parameter vector is defined by $\boldsymbol{\mu} = \{x_0,y_0,\Delta_x,\Delta_y,R\}$. The cross-section function for the rectangle is

$$\sigma(u, v) = \begin{cases} 0 & u_1 < u < u_2 \text{ and } v_1 < v < v_2, \\ 1 & \text{otherwise,} \end{cases}$$

where $u_1=\frac{x_0-\Delta_x}{\sqrt{2\lambda R}}$, $u_2=\frac{x_0+\Delta_x}{\sqrt{2\lambda R}}$, $v_1=\frac{y_0-\Delta_y}{\sqrt{2\lambda R}}$, and $v_2=\frac{y_0+\Delta_y}{\sqrt{2\lambda R}}$ are the scaled coordinates that correspond to the four edges of the rectangle. Substituting (7) into (4) and (5), we arrive at exact formulas for the gain functions of rectangular screen as follows:

$$f_c(u',v') = \frac{1}{2} S(u',u_1,u_2) S(v',v_1,v_2)$$

$$-\frac{1}{2} C(u',u_1,u_2) C(v',v_1,v_2), \qquad (8)$$

$$f_s(u',v') = 1 - \frac{1}{2} S(u',u_1,u_2) C(v',v_1,v_2)$$

$$-\frac{1}{2} C(u',u_1,u_2) S(v',v_1,v_2), \qquad (9)$$

where $C(z',z_1,z_2) = C(z_2-z') + C(z'-z_1)$, $S(z',z_1,z_2) = S(z_2-z') + S(z'-z_1)$, $C(z) = \int_0^z \cos\left(\frac{\pi}{2}\,t^2\right) \mathrm{d}t$, and $S(z) = \int_0^z \sin\left(\frac{\pi}{2}\,t^2\right) \mathrm{d}t$ are the Fresnel integrals.

In Fig. 3(b), we plot the amplitude of the received signal gain along x-axis for rectangles with widths $\Delta_x=0.5$ and 0.25 m for a case with a carrier of 10 GHz and a blockage range of R=2 m. It can be observed that the gain variation pattern critically depends on the size of the rectangular blockage, especially for the region between the shadow edges.

IV. CRAMER-RAO BOUND ANALYSIS

In the previous section, we illustrated how the common environmental parameters μ affect the gain variation of the received signal through the array steering matrix $A(\theta, \mu)$. Based on the model in (1), joint source DoA and blockage range estimation can be performed by maximizing the proper maximum likelihood (ML) function. In this section, we analyze the performance of maximum likelihood estimation for both deterministic and stochastic ML signal models by deriving the corresponding CRBs. One of the key differences between this work and existing CRB analyses is that we consider both the source dependent parameters θ and environmental parameters μ that are common to all source signals. Mathematically speaking, the DoA of the kth source only appears in the kth column of A, while the common parameters affect all the elements in A. In the following, we first introduce the two types of models used for maximum likelihood estimation. Then, we derive the CRBs for both cases.

A. Deterministic and Stochastic ML Models

The so-called deterministic or conditional model assumes the source signals, $\mathbf{x}(t)$, to be nonrandom parameters to

be estimated [4]. Based on (1), this results in $\mathbf{s}(t) \sim \mathcal{CN}(\mathbf{A}(\boldsymbol{\theta}, \boldsymbol{\mu})\mathbf{x}(t), \sigma\mathbf{I}_M)$. In contrast, the stochastic or unconditional model assumes the signals to be random such that $\mathbf{s}(t) \sim \mathcal{CN}(0, \mathbf{R}_s)$ where $\mathbf{R}_s = \mathbf{A}\mathbf{R}_x\mathbf{A}^H + \sigma\mathbf{I}_M$ and \mathbf{R}_x is the covariance matrix of the transmitted signals \mathbf{x} .

B. CRB Analysis for the Deterministic ML Model

The likelihood function of the data in this case is

$$L(\boldsymbol{\theta}, \boldsymbol{\mu}, \mathbf{x}) = \frac{1}{(\pi \sigma^2)^{MN}} \exp\left(-\frac{1}{\sigma^2} \sum_{t=1}^{N} \|\mathbf{s}_t - \mathbf{A}\mathbf{x}_t\|^2\right),$$
(10)

where $\mathbf{x}_t = [x_1(t), \cdots, x_K(t)]^T$ is the transmitted signal at snapshot t and N is the total number of snapshots. We assume there are K DoAs and T common parameters. Since θ_k only appears in the kth column of the steering matrix \mathbf{A} , the derivative of \mathbf{A} with respect to the DoAs can be written as the $M \times K$ matrix $\mathbf{D}_{\theta} = [\frac{\partial \mathbf{a}(\theta_1, \boldsymbol{\mu})}{\partial \theta_1}, \cdots, \frac{\partial \mathbf{a}(\theta_K, \boldsymbol{\mu})}{\partial \theta_K}]$. For the common parameters, we denote $\mathbf{D}_{\mu_{\tau}} = [\frac{\partial \mathbf{a}(\theta_1, \boldsymbol{\mu})}{\partial \mu_{\tau}}, \cdots, \frac{\partial \mathbf{a}(\theta_K, \boldsymbol{\mu})}{\partial \mu_{\tau}}]$, where $\tau \in \{1, 2, \cdots, T\}$, and we stack these matrices to form the $M \times KT$ matrix $\mathbf{D}_{\mu} = [\mathbf{D}_{\mu_1}, \cdots, \mathbf{D}_{\mu_T}]$. For notational convenience, we further define the following signal matrices: $\mathbf{X}_t = \mathrm{diag}\{x_1(t), \cdots, x_K(t)\}$ and $\mathbf{Y}_t = \mathbf{I}_T \otimes \mathbf{x}_t$. The key result of this section is contained in the follow theorem.

Theorem 1. For the deterministic ML model, the CRBs for source DoAs θ and common parameters μ are given by

$$CRB^{-1}(\boldsymbol{\theta}) = \frac{2}{\sigma} \sum_{t}^{N} Re \left[\mathbf{X}_{t}^{*} \mathbf{D}_{\theta}^{*} \mathbf{P}_{A}^{\perp} \mathbf{D}_{\theta} \mathbf{X}_{t} - \mathbf{C}_{\theta\mu} (\mathbf{Y}_{t}^{*} \mathbf{D}_{\mu}^{*} \mathbf{P}_{A}^{\perp} \mathbf{D}_{\mu} \mathbf{Y}_{t})^{-1} \mathbf{C}_{\theta\mu}^{*} \right],$$
(11)

$$CRB^{-1}(\boldsymbol{\mu}) = \frac{2}{\sigma} \sum_{t}^{N} Re \left[\mathbf{Y}_{t}^{*} \mathbf{D}_{\mu}^{*} \mathbf{P}_{A}^{\perp} \mathbf{D}_{\mu} \mathbf{Y}_{t} - \mathbf{C}_{\theta \mu} (\mathbf{X}_{t}^{*} \mathbf{D}_{\theta}^{*} \mathbf{P}_{A}^{\perp} \mathbf{D}_{\theta} \mathbf{X}_{t})^{-1} \mathbf{C}_{\theta \mu}^{*} \right],$$
(12)

where $\mathbf{P}_{A}^{\perp} = \mathbf{I} - \mathbf{A}(\mathbf{A}^*\mathbf{A})^{-1}\mathbf{A}^*$ and $\mathbf{C}_{\theta\mu} = \frac{2}{\sigma}\sum_{t}^{N} \operatorname{Re}\left[\mathbf{X}_{t}^{*}\mathbf{D}_{\theta}^{*}\mathbf{P}_{A}^{\perp}\mathbf{D}_{\mu}\mathbf{Y}_{t}\right].$

Proof. See Appendix A.
$$\Box$$

C. CRB Analysis for the Stochastic ML Model

A key drawback of the deterministic ML model is that the CRB cannot in general be asymptotically achieved as $N \to \infty$, since the dimension of the signal parameters to be estimated grows linearly with N and consistent estimates of the signal parameters cannot be obtained. As a result, when applicable the stochastic ML approach is preferred since in general it is statistically efficient. In this case, we assume a known source signal covariance and the likelihood function is given by:

$$L(\boldsymbol{\theta}, \boldsymbol{\mu}) = \frac{1}{\pi^M \det(\mathbf{R}_s)} \exp\left(-\sum_{t=1}^N \mathbf{s}_t^{\mathrm{H}} \mathbf{R}_s^{-1} \mathbf{s}_t\right).$$
(13)

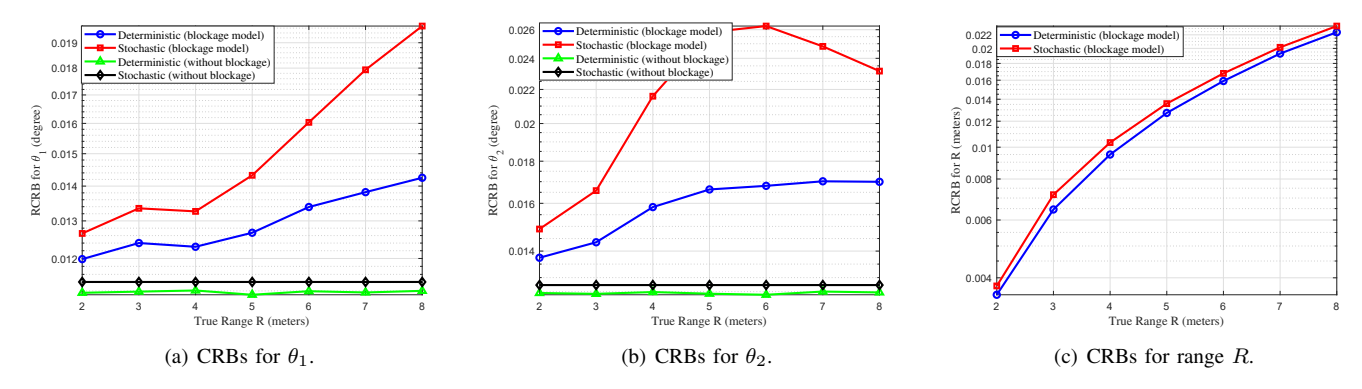


Fig. 4. Root CRB (RCRB) versus true range for the blockage (proposed) and blockage-free (conventional) models.

From [4, (2.10)], the Fisher information matrix (FIM) for this case is given by:

$$FIM = \begin{bmatrix} \mathbf{F}_{\theta\theta} & \mathbf{F}_{\theta\mu} \\ \mathbf{F}_{\mu\theta} & \mathbf{F}_{\mu\mu} \end{bmatrix}$$
 (14)

with elements $\operatorname{FIM}_{i,j} = N\operatorname{Tr}\left[\mathbf{R}_s^{-1}\frac{\partial\mathbf{R}_s}{\partial\boldsymbol{\phi}_i}\mathbf{R}_s^{-1}\frac{\partial\mathbf{R}_s}{\partial\boldsymbol{\phi}_j}\right]$ and where we define $\boldsymbol{\phi} = [\boldsymbol{\theta}, \boldsymbol{\mu}]^T$. Denoting the $M^2 \times K$ matrix $\tilde{\mathbf{D}}_{\boldsymbol{\theta}} = \left[\operatorname{vec}\left(\frac{\partial\mathbf{R}_s}{\partial\theta_1}\right), \operatorname{vec}\left(\frac{\partial\mathbf{R}_s}{\partial\theta_2}\right), \cdots, \operatorname{vec}\left(\frac{\partial\mathbf{R}_s}{\partial\theta_K}\right)\right]$, the $M^2 \times T$ matrix $\tilde{\mathbf{D}}_{\boldsymbol{\mu}} = \left[\operatorname{vec}\left(\frac{\partial\mathbf{R}_s}{\partial\mu_1}\right), \operatorname{vec}\left(\frac{\partial\mathbf{R}_s}{\partial\mu_2}\right), \cdots, \operatorname{vec}\left(\frac{\partial\mathbf{R}_s}{\partial\mu_T}\right)\right]$, and using the identity $\operatorname{Tr}(\mathbf{A}\mathbf{B}\mathbf{C}^\top) = \operatorname{vec}(\mathbf{C})^\top(\mathbf{I}\otimes\mathbf{A})\operatorname{vec}(\mathbf{B})$, we can explicitly write the FIM submatrices as follows:

$$\mathbf{F}_{\theta\theta} = 2N \cdot \operatorname{Re}\left(\tilde{\mathbf{D}}_{\theta}^{\mathrm{H}}\left(\mathbf{R}_{s}^{-1} \otimes \mathbf{R}_{s}^{-1}\right)\tilde{\mathbf{D}}_{\theta}\right),\tag{15}$$

$$\mathbf{F}_{\mu\mu} = 2N \cdot \text{Re} \left(\tilde{\mathbf{D}}_{\mu}^{\text{H}} \left(\mathbf{R}_{s}^{-1} \otimes \mathbf{R}_{s}^{-1} \right) \tilde{\mathbf{D}}_{\mu} \right), \tag{16}$$

$$\mathbf{F}_{\theta\mu} = \mathbf{F}_{\mu\theta} = 2N \cdot \text{Re} \left(\tilde{\mathbf{D}}_{\theta}^{\text{H}} \left(\mathbf{R}_{s}^{-1} \otimes \mathbf{R}_{s}^{-1} \right) \tilde{\mathbf{D}}_{\mu} \right).$$
 (17)

Finally, using the Schur complement of the FIM matrix in (14), we arrive at the following theorem.

Theorem 2. For the stochastic ML model, the CRBs for the source DoAs θ and common parameters μ are

$$CRB^{-1}(\boldsymbol{\theta}) = \frac{2N}{\sigma} Re \left[\tilde{\mathbf{D}}_{\boldsymbol{\theta}}^{H} \left(\mathbf{R}_{s}^{-1} \otimes \mathbf{R}_{s}^{-1} \right) \tilde{\mathbf{D}}_{\boldsymbol{\theta}} - \mathbf{F}_{\boldsymbol{\theta}\mu} (\tilde{\mathbf{D}}_{\mu}^{H} \left(\mathbf{R}_{s}^{-1} \otimes \mathbf{R}_{s}^{-1} \right) \tilde{\mathbf{D}}_{\boldsymbol{\mu}})^{-1} \mathbf{F}_{\boldsymbol{\theta}\mu}^{*} \right],$$
(18)

$$CRB^{-1}(\boldsymbol{\mu}) = \frac{2N}{\sigma} Re \left[\tilde{\mathbf{D}}_{\boldsymbol{\mu}}^{H} \left(\mathbf{R}_{s}^{-1} \otimes \mathbf{R}_{s}^{-1} \right) \tilde{\mathbf{D}}_{\boldsymbol{\mu}} - \mathbf{F}_{\theta \boldsymbol{\mu}} (\tilde{\mathbf{D}}_{\theta}^{H} \left(\mathbf{R}_{s}^{-1} \otimes \mathbf{R}_{s}^{-1} \right) \tilde{\mathbf{D}}_{\theta})^{-1} \mathbf{F}_{\theta \boldsymbol{\mu}}^{*} \right].$$
(19)

Proof. The proof is relegated to future work.

V. NUMERICAL RESULTS

In this section, we numerically evaluate the CRBs for the deterministic and stochastic models and implement ML estimators of the source DoA and blockage range. We consider the simple scenario depicted in Fig. 5 where two far-field sources with DoAs θ_1 and θ_2 transmit signals to a uniform linear array with M=41 antenna elements. The true DoAs are

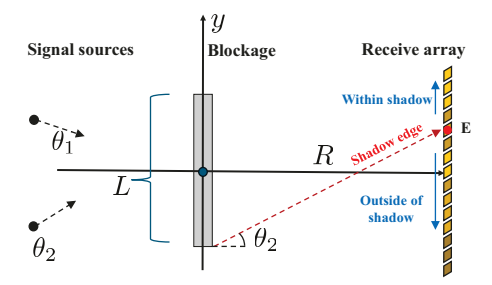


Fig. 5. Set up for the numerical study.

set as $\theta_1=15^\circ$ and $\theta_2=-30^\circ$. The carrier frequency of the signal is $f_c=5.9$ GHz and the size of the blockage is L=0.5 m. The receive array is linear with uniformly spaced elements of one-half wavelength spacing, and thus the total aperture is D=1 m. In the following simulations, we consider a blockage-free scenario as the baseline. For this case, the signal model is simply given by $\mathbf{s}(t)=[\mathbf{a}_0(\theta_1),\mathbf{a}_0(\theta_2)]\cdot\mathbf{x}(t)+\mathbf{n}(t),$ where $\mathbf{a}(\theta)=[1,e^{j\pi\sin\theta},\cdots,e^{j(M-1)\pi\sin\theta}]^T$ is the far-field array steering vector.

A. CRB versus true blockage range

In Fig. 4, we compare the CRBs for the given scenarios with and without the blockage. For each case, we further compare the CRBs for the deterministic and stochastic signal models. From Fig. 4(a) and (b), we can see that the presence of the blockage significantly increases the CRBs for DoA estimation. This is because a substantial portion of the received signal energy does not receive the array and thus the effective signal-to-noise ratio is lower compared with the blockage-free scenario. In addition, we note that the deterministic model always gives a more optimistic CRB result compared to the stochastic model. Interestingly, the stochastic CRB for θ_2 first increases with R, reaches a peak value at R=6, then begins to decrease for larger R. This can be explained by inspecting the shadow edge of the blockage. In Fig. 5, we use E to denote the edge of the shadow cast on the receive array by the second source. As R increase, E will move towards the top edge of the array. When R is sufficiently large, the entire array will be outside of the shadow. In other words, the blockage is moving

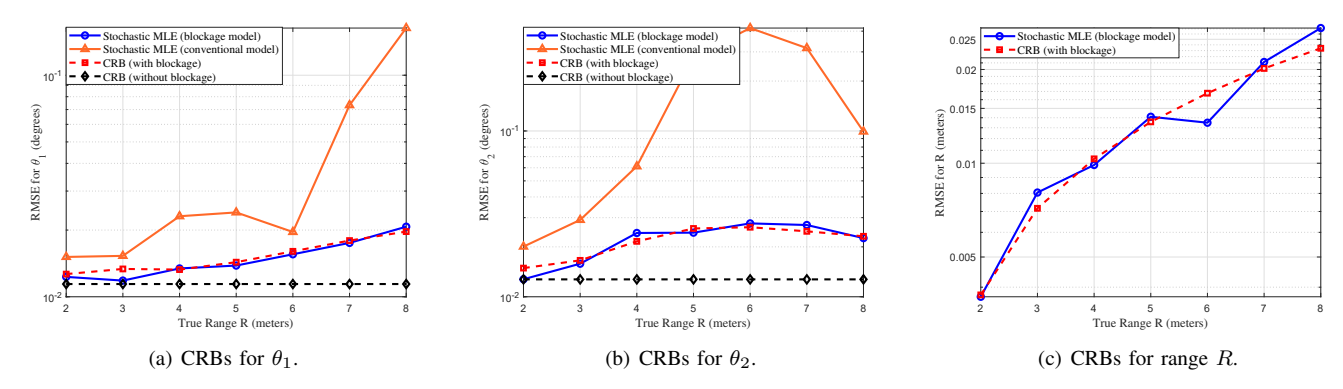


Fig. 6. RMSEs for the stochastic MLE under blockage (proposed) and blockage-free (conventional) models.

outside of the first few Fresnel zones [6] of the line-of-sight channel and thus the blockage has a smaller impact on the received signal. In Fig. 4(c), we see that the deterministic and stochastic CRBs for the range estimate are similar and increase R. This results because the diffraction effects that are critical for determining R become weaker as the distance between the array and the blockage increases.

B. Comparison of ML estimates with CRBs

To demonstrate near-field sensing capabilities, we optimize the ML criterion to obtain estimates for θ_1 , θ_2 , and R using the stochastic ML model in (13). The signal model derived in (3), (8), and (9) allows us to find the analytical derivatives of the likelihood function with respect to the parameters of interest, and we then use Newton's method to implement a simple 3-dimensional search for the parameters. In Fig. 6(a) and (b) we plot the root mean square error (RMSE) of the ML DoA estimates versus R for the case where the blockage is taken into account and also when its presence is ignored. The stochastic CRBs for the cases with and without a blockage are also provided. We observe that the performance of the ML estimates generally matches the CRB, while ignoring the blockage leads to considerable degradation in the DoA estimates. This demonstrates the importance of incorporating blockage parameters μ into the signal model and the ability to conduct near-field sensing with the appropriate signal model.

VI. CONCLUSIONS

We have proposed a diffraction-based model for partially-blocked channels that analytically captures the effects of signal diffraction in the array steering vectors in closed-form. We presented two case studies where the range and size parameters of the blockage are explicitly modeled in the array steering vector. Based on the proposed model, we analyzed the performance of maximum likelihood estimation for both deterministic and stochastic ML signal models by deriving the corresponding CRBs. Finally, we numerically evaluated the derived CRBs and compared them with the RMSE of the maximum likelihood estimates obtained by multi-dimensional Newton's search. Simulations revealed that the CRB of the range estimates steadily increases as the diffraction effects

weaken, and the CRB of DoA estimates largely depends on the proportion of receive antennas that fall within the shadowed region created by the blockage.

APPENDIX A PROOF OF **THEOREM 1**

Based on the likelihood function given in (10), we write the FIM as FIM = $\mathbb{E}\left[\left(\frac{\partial \ln L}{\partial \psi}\right)\left(\frac{\partial \ln L}{\partial \psi}\right)^T\right]$, where $\psi = \left[\bar{x}_1, \tilde{x}_1, \cdots, \bar{x}_N, \tilde{x}_N, \boldsymbol{\theta}^T, \boldsymbol{\mu}^T\right]^T$ is the vector containing the source and blockage parameters as well as the signal samples over the N snapshots. Here, we use \bar{x} and \tilde{x} to denote the real and imaginary part of x, respectively. Similarly, we define $\bar{\mathbf{H}} = \frac{2}{\sigma} \mathrm{Re}\{\mathbf{A}^*\mathbf{A}\}$ and $\tilde{\mathbf{H}} = \frac{2}{\sigma} \mathrm{Imag}\{\mathbf{A}^*\mathbf{A}\}$. Using the notation above and the results given in [3], we have

$$\mathrm{FIM} = \begin{bmatrix} \bar{\mathbf{H}} & -\tilde{\mathbf{H}} & 0 & \cdots & 0 & \bar{\Delta}_1 \\ \tilde{\mathbf{H}} & \bar{\mathbf{H}} & 0 & \cdots & 0 & \bar{\Delta}_1 \\ 0 & \bar{\mathbf{H}} & -\tilde{\mathbf{H}} & \cdots & 0 & \bar{\Delta}_2 \\ 0 & \tilde{\mathbf{H}} & \bar{\mathbf{H}} & \cdots & 0 & \bar{\Delta}_2 \\ \vdots & \vdots & \ddots & \vdots & \vdots \\ 0 & 0 & \cdots & \bar{\mathbf{H}} & -\tilde{\mathbf{H}} & \bar{\Delta}_N \\ \bar{\Delta}_1^T & \bar{\Delta}_1^T & \bar{\Delta}_2^T & \bar{\Delta}_2^T & \cdots & \bar{\Delta}_N^T & \bar{\Delta}_N^T & \Gamma \end{bmatrix},$$

$$(A.1)$$

where Γ contains the FIM elements for θ and μ , and we define the $K \times (K+T)$ matrix $\Delta_t = [\frac{2}{\sigma} \mathbf{A}^* \mathbf{D}_{\theta} \mathbf{X}_t, \frac{2}{\sigma} \mathbf{A}^* \mathbf{D}_{\mu} \mathbf{Y}_t]$. Finally, using the Schur complement for matrix inversion, the CRBs for θ and μ can be obtained.

REFERENCES

- [1] Y. Han, S. Jin, M. Matthaiou, T. Q. S. Quek, and C.-K. Wen, "Toward extra large-scale MIMO: New channel properties and low-cost designs," *IEEE Internet Things J.*, vol. 10, no. 16, pp. 14569–14594, 2023.
- [2] E. De Carvalho, A. Ali, A. Amiri, M. Angjelichinoski, and R. W. Heath, "Non-stationarities in extra-large-scale massive MIMO," *IEEE Wireless Commun.*, vol. 27, no. 4, pp. 74–80, Aug. 2020.
- [3] P. Stoica and A. Nehorai, "Music, maximum likelihood, and Cramer-Rao bound," *IEEE Transactions on Acoustics, Speech, and Signal Processing*, vol. 37, no. 5, pp. 720–741, 1989.
- [4] —, "Performance study of conditional and unconditional direction-ofarrival estimation," *IEEE Transactions on Acoustics, Speech, and Signal Processing*, vol. 38, no. 10, pp. 1783–1795, 1990.
- [5] M. Born and E. Wolf, Principles of optics: Electromagnetic Theory of Propagation, Interference and Diffraction of Light. Elsevier, 2013.
- [6] R. E. Sheriff, "Understanding the Fresnel zone," AAPG Explorer, pp. 18–19, 1996.